

1 Article

2 Optical, dielectric and magnetic properties of 3 $\text{La}_{1-x}\text{Nd}_x\text{FeO}_3$ powders and ceramics

4 Paweł Głuchowski ^{1,2,*}, Karen Oganisian ¹, Robert Tomala ¹, Anna Łukowiak ¹,
5 Dmitry Karpinsky ³, Denis Alikin ^{4,5}, Andrei Kholkin ⁴, Wiesław Stręk ¹

6 ¹ Institute of Low Temperature and Structure Research, PAS, PL-50422 Wrocław, Poland; intibs@intibs.pl,

7 ² Nanoceramics Inc, PL-50422 Wrocław, Poland; office@nanoceramics.pl

8 ³ Scientific and Practical Materials Research Center NAS Belarus, BY-220072 Minsk, Belarus,
9 ifttpanb@ifttp.bas-net.by

10 ⁴ Physics Dept and CICECO - Aveiro Institute of Materials of &, University of Aveiro, PT-3810-193 Aveiro,
11 Portugal

12 ⁵ School of Natural Sciences and Mathematics, Ural Federal University, 620000 Ekaterinburg, Russia

13 * Correspondence: p.gluchowski@intibs.pl; Tel.: +48-71-395-4174

14

15 **Abstract:** Nanocrystalline $\text{La}_{1-x}\text{Nd}_x\text{FeO}_3$ powders with different concentrations of Nd^{3+} have been
16 synthesized by modified Pechini method. Their structure was studied by X-ray powder diffraction
17 (XRD). Further, $\text{La}_{1-x}\text{Nd}_x\text{FeO}_3$ nanoceramics were prepared by high pressure sintering technique.
18 The luminescence spectra of the powders were investigated as a function of concentration of active
19 dopant to check the possible energy transfers observed due to Nd^{3+} concentration changes. The
20 electrical and magnetic properties of the powders and ceramics were investigated to determine the
21 effect of Nd^{3+} doping on the dielectric permittivity and magnetization in the wide frequency range.

22 **Keywords:** perovskites, neodymium, luminescence, electric transport, magnetization

23

24 1. Introduction

25 The LaFeO_3 (LFO) perovskite series have been extensively studied for their interesting physical
26 properties and potential applications in catalysis, solid oxide fuel cells, permeation membranes,
27 ultrasensitive magnetic read heads, gas sensors, interconnecting materials for the solar cells, and
28 magnetic memory elements [1, 2]. One of the most studied properties of rare-earth (RE) orthoferrites,
29 REFeO_3 , are their unique magnetic responses, such as spin reorientation, spin canting, ultra-fast spins
30 switching, magneto-optics, and magnetization reversal [3-6]. Spin reorientation is closely related to
31 excellent coupling between electric and magnetic degrees of order, and this coupling is very
32 important to search for the novel magneto-electric multiferritics [7]. Another interesting properties
33 of such perovskites is due to their use as a proton-conductive material for efficient negative-electrode
34 for Ni-MH batteries [8]. Among the rare-earth perovskite orthoferrites LFO is a very well-known
35 canted antiferromagnetic insulator with an orthorhombically distorted perovskite structure (contain
36 only trivalent iron and exhibiting a high value of the Néel temperature ($T_N \sim 740$ K) [9]. Although a
37 number of papers, related to the structural and magnetic properties of LFO, has been reported [10,
38 11], only few present multiferroic behavior in LFO [12].

39 Substitution of lanthanum ions with other RE elements having smaller ionic radii leads to a
40 shrinkage of the unit cell accompanied with a modification of the oxygen octahedral rotation and
41 corresponding changes in the length and angles of Fe–O chemical bonds. Notable changes in the
42 structural parameters lead to a modification of magnetic, dielectric, transport, and optical properties
43 of the doped compounds. Doping with neodymium ions, which have small difference in the ionic
44 radii with lanthanum ions, allows controlling structural parameters and manipulating physical
45 properties of the LaFeO_3 -based compounds.

46 Application potential of REFeO₃ compounds depends strongly on their electric, magnetic, and
47 optical properties. Therefore, it is important to study the influence of different parameters on the
48 materials' characteristic. For example nanoparticles may show unusual magnetic properties due to
49 the finite-size effects, surface anisotropy effects, interface effects or shape anisotropy effect [13],
50 therefore it is interesting to study also ceramics composed of nanograins. Here, we discuss the
51 properties of LaFeO₃ nanocrystals and nanoceramics varied with Nd³⁺ ions doping.

52 2. Materials and Methods

53 Nanocrystalline La_{1-x}Nd_xFeO₃ powders with different concentrations of Nd³⁺ ($x = 0 \div 0.1$) have
54 been synthesized by modified Pechini method [14]. The material was prepared by dissolving the
55 stoichiometric amount of La₂O₃ (Sigma-Aldrich, 99.9%) and Nd₂O₃ (Sigma Aldrich, 99.9%) in HNO₃
56 (POCH, 65% analytical grade) to obtain RE nitrates. To eliminate nitric acid, nitrates were dissolved
57 in the deionized water and evaporated three times. The RE nitrates, Fe(NO₃)₃•9H₂O (Sigma Aldrich,
58 99.95%), citric acid (CA) (Sigma Aldrich, 99%), and ethylene glycol (Sigma Aldrich, 99.8%) were
59 dissolved in deionized water. The stoichiometric molar ratio of metal ions to CA was 1:5. The
60 mixtures were continuously stirred for 1 h and then transferred to a dryer. The temperature was kept
61 at 80 °C. After one week, the sol formed brown resin that was transferred to the crucibles and fired
62 at 850 °C in a furnace for 8 h. The powder products were grinded in the agate mortar and taken to
63 the analysis and ceramic sintering process. The details of the ceramic sintering process based on the
64 high pressure technique was reported elsewhere [15]. Briefly, LaFeO₃ and La_{1-x}Nd_xFeO₃ powders
65 were formed in pellets under the pressure of 0.1 GPa at room temperature. The pellets were placed
66 in a special shape container with a resistance heater and separated by boron nitride layers. The force
67 exerted by the anvils produced quasi-isostatic pressure of 8 GPa and the ceramic was sintered at
68 500 °C.

69 Structural studies were performed by powder X-ray diffraction (XRD) using a PANalytical
70 X'Pert diffractometer with Ni-filtered Cu K α radiation, $\lambda=0.15418$ nm. Atomic force microscopy
71 (AFM) methods were used to inspect grain structure of ceramics and their compositional
72 homogeneity. AFM was done using commercial scanning probe microscope Ntegra Aura (NT-MDT
73 Spectral Instruments, Russia) by Budget Sensors ElectriTap300-G tips with the curvature less 25 nm,
74 resonance frequency about 300 kHz, and 20 N/m force constant. In order to clarify chemical
75 homogeneity at the local scale we used Kelvin probe force microscopy (KPFM) allowing direct
76 inspection of the work function distribution across the surface with high spatial resolution [16]. The
77 possible secondary phases would result in an apparent variation of electronic structure and work
78 function. KPFM was done using conventional two-pass approach with 2 V ac voltage applied to the
79 tip and 50 nm lift distance.

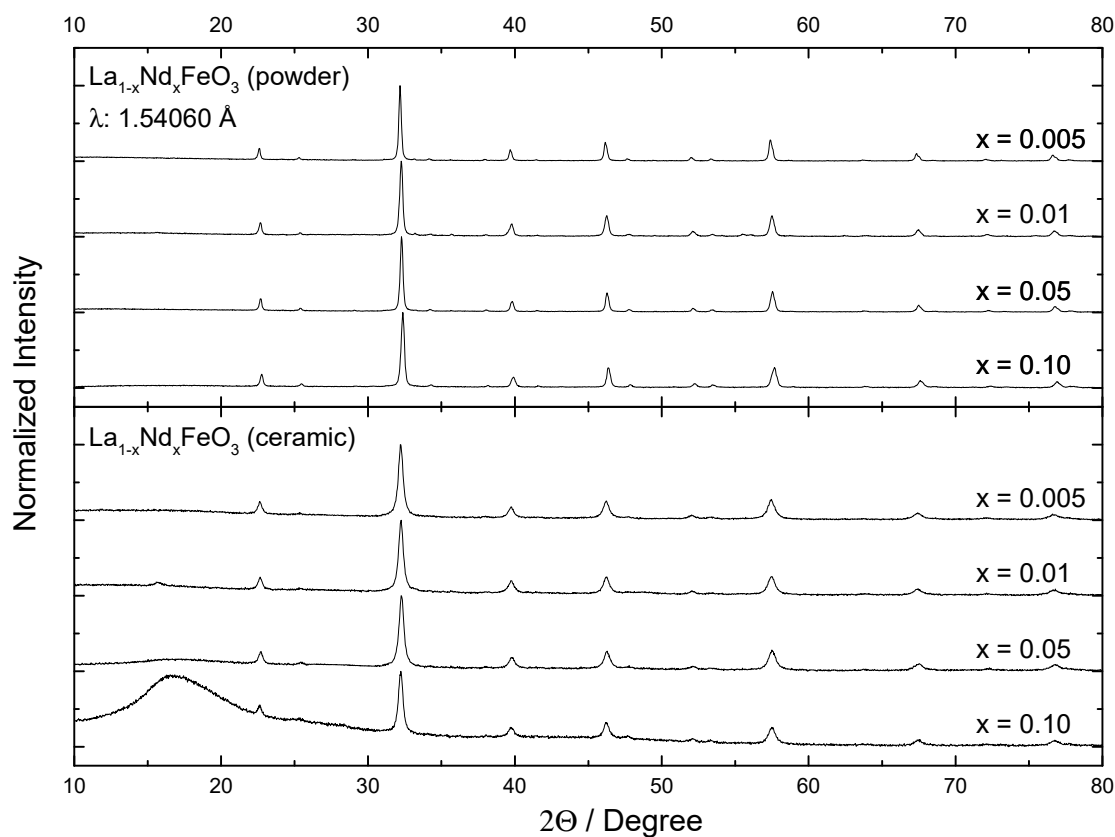
80 Optical properties of the powders doped with Nd³⁺ ions were studied with Renishaw
81 Microscope equipped with CCD camera (0.1 nm resolution), 2400 line/mm gratings and argon laser
82 as an excitation source (λ_{exc} : 514 nm, 100 mW). Electric impedance was measured using Alpha
83 analyser (Novocontrol GmbH) with active sample cell operating in a frequency range 10⁻² - 10⁶ Hz at
84 room temperature with ac voltage amplitude of 0.1 V. The measured sample was supplied with gold
85 electrodes. Isothermal magnetization measurements were performed in magnetic fields up to +/-14 T
86 at 5 and 300 K using Physical Properties Measurement Systems from Cryogenic Ltd.

87 3. Results

88 3.1. Structure and morphology

89 LaFeO₃ is an orthorhombically distorted perovskite structure with space group Pbnm [17]. XRD
90 patterns of all powders were consistent with the orthorhombic structure of LaFeO₃ in the standard
91 from JCPDS 88-0641 (Fig. 1). The average crystallite sizes and cells parameters of all samples were
92 calculated from X-ray line broadening of the peaks using Rietveld Refinement in X'Pert HighScore
93 Plus software and are presented in Table 1. All samples have crystallites below 100 nm and

94 microstrains of about 0.02%. With increasing Nd content we observed shortening of the *b* and *c* axes
 95 in the crystallites. This suggests that the distances between the ions located along [010] and [001]
 96 directions decreases. It is interesting that after applying pressure during sintering the peaks are
 97 broadened due to decrease of grain size and microstrains increased. The broad band observed about
 98 18 degree for La_{0.9}Nd_{0.1}FeO₃ ceramic is related to the amorphous phase of the nanocrystal located on
 99 the surface of the grains. This behavior was observed also for other ceramics prepared from
 100 nanocrystals and it is related to the decomposition of the surface of nanocrystals and increase of the
 101 strains on the grain boundaries [18].



102

103 **Figure 1.** XRD of the La_{1-x}Nd_xFeO₃ powders and ceramics doped with different concentration of
 104 Nd³⁺

105

Table 1. Cell parameters and crystallite sizes of the La_{1-x}Nd_xFeO₃ powders and ceramics.

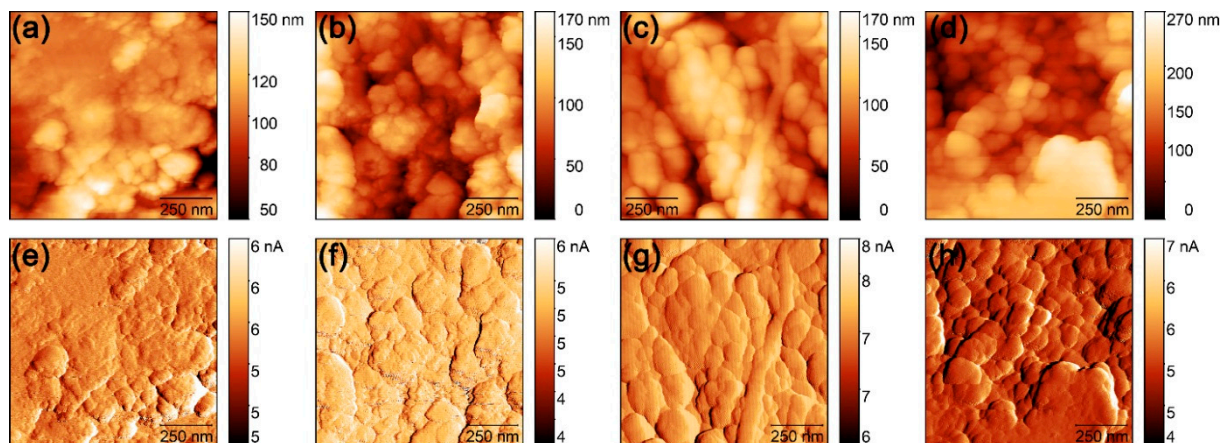
La _{1-x} Nd _x FeO ₃	Crystallite size / nm	<i>a</i>	<i>b</i>	<i>c</i>	Strains / %
powder					
x = 0.005	67	5.5633(2)	7.8510(3)	5.5529(9)	0.021
x = 0.01	52	5.5709(1)	7.8450(0)	5.5480(6)	0.021
x = 0.05	61	5.5657(6)	7.8448(7)	5.5447(0)	0.019
x = 0.10	50	5.5666(8)	7.8375(7)	5.5364(8)	0.022
ceramic					
x = 0.005	24	5.5656(9)	7.8833(4)	5.5339(7)	0.045
x = 0.01	25	5.5658(7)	7.8825(6)	5.5351(9)	0.042
x = 0.05	24	5.5625(3)	7.8780(2)	5.5333(5)	0.044
x = 0.10	30	5.5628(0)	7.8689(0)	5.5251(6)	0.044

106

107

Nano size of the grains in the ceramics are confirmed by AFM images (Fig. 2). The average grain size in ceramics was about 20-30 nm and gradually increased with Nd³⁺ doping. Most of the compositions

108 had quite dense structure without significant amount of pores. KPFM analysis showed high quality
 109 homogeneity of all compositions (see supplementary, Figure S1). The only variation of contact
 110 potential difference was found at the grain boundaries, which can be attributed to typical artifacts of
 111 KPFM measurements [16]. Measured contact potential difference values increased slightly with
 112 doping due to apparent variation of the electronic structure of material with composition.

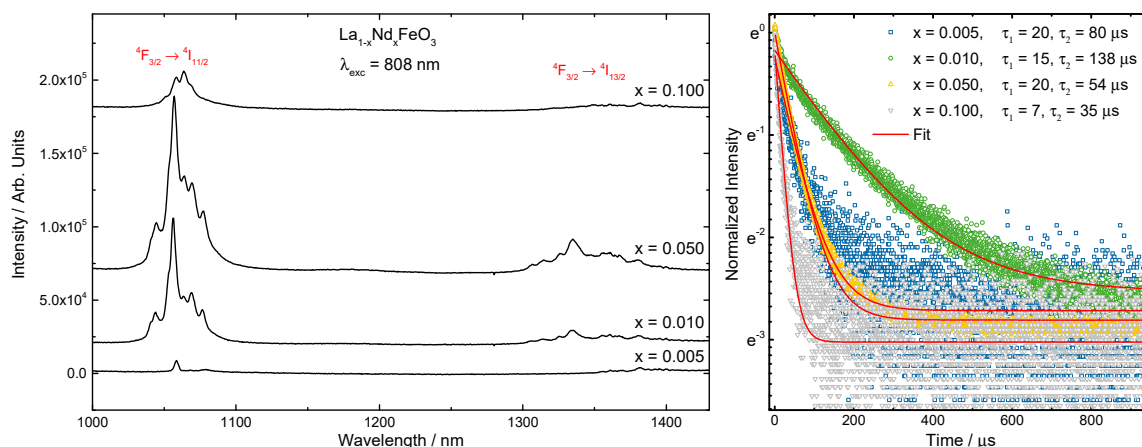


113
 114 **Figure 2.** (a)-(d) Topography and (e)-(h) deflection signal (differential topography) of $\text{La}_{1-x}\text{Nd}_x\text{FeO}_3$ ceramics in dependence of Nd doping degree. (a), (e) 0.5%; (b), (f) 1%; (c), (g) 5%;
 115 (d), (h) 10%.

117 3.2. Optical properties

118 The Nd^{3+} concentration dependence of photoluminescence of $\text{La}_{1-x}\text{Nd}_x\text{FeO}_3$ nanocrystals was
 119 measured at room temperature (Fig. 3). The observed luminescence bands at 1057 and 1335 nm
 120 were assigned to the ${}^4\text{F}_{3/2} \rightarrow {}^4\text{I}_{11/2}$ and ${}^4\text{F}_{3/2} \rightarrow {}^4\text{I}_{13/2}$ transitions of Nd^{3+} , respectively. Figure 3 shows
 121 the effect of Nd^{3+} ions concentration on luminescence spectra and suggests that concentration
 122 quenching effects took place when doped with 10 mol-% of Nd^{3+} ions. Low emission intensity and
 123 unexpected shorter decay time of the $\text{La}_{0.995}\text{Nd}_{0.005}\text{FeO}_3$ nanocrystals is related low concentration
 124 of the Nd ions and high absorption of the material (dark brown color). The concentration
 125 quenching is related to the different ion distances between donors and acceptors and smaller
 126 separation between pairs. For Nd^{3+} ion-ion energy transfer is generally described on the basis of
 127 dipole-dipole interactions. The processes involved in cross-relaxation are ${}^4\text{F}_{3/2}, {}^4\text{I}_{9/2} \rightarrow {}^4\text{I}_{15/2}, {}^4\text{I}_{15/2}$,
 128 and/or ${}^4\text{F}_{3/2}, {}^4\text{I}_{9/2} \rightarrow {}^4\text{I}_{13/2}, {}^4\text{I}_{15/2}$; and in energy migration is ${}^4\text{F}_{3/2}, {}^4\text{I}_{9/2} \rightarrow {}^4\text{I}_{9/2}, {}^4\text{F}_{3/2}$. Additional process
 129 that lead to the quenching of the luminescence is the thermalization effect that is strengthened
 130 by the small size of the grains (due to inefficient removal of heat) and resulted in enhancement
 131 of local temperature in individual grains. The concentration quenching have been confirmed by
 132 measurement of kinetics of Nd^{3+} emission. The decay time of emission from ${}^4\text{F}_{3/2}$ level decreases
 133 significantly when dopant concentration is higher than 1 mol%. For the ceramics,
 134 photoluminescence measurements were impossible to be performed due to black color of the
 135 ceramics after sintering and total absorption of the visible excitation light.

136

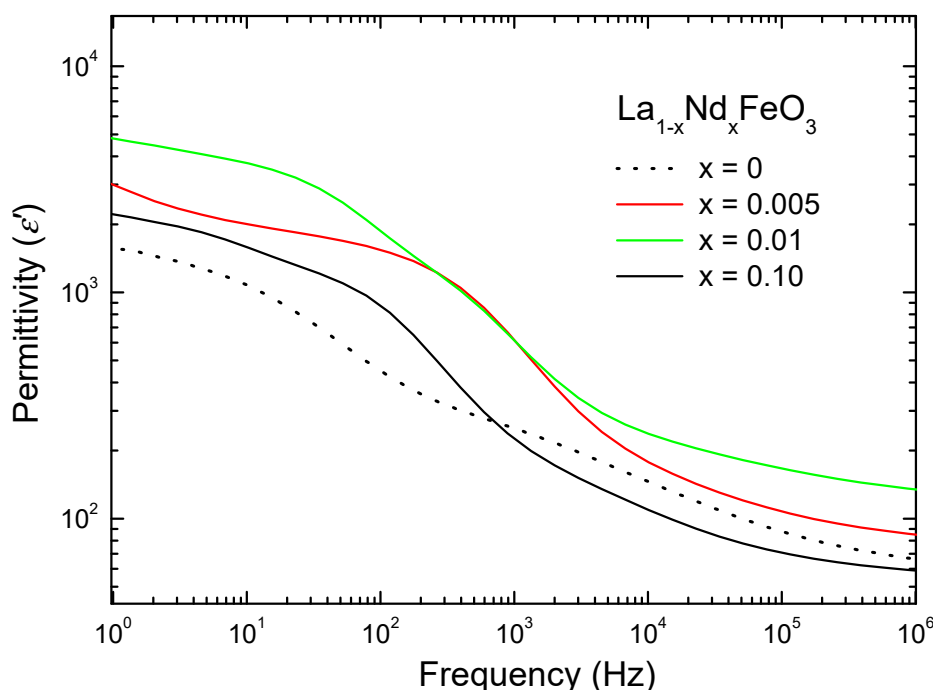


137

138 **Figure 3.** NIR luminescence of the $\text{La}_{1-x}\text{Nd}_x\text{FeO}_3$ powders under 808 LD excitation (left) and the
 139 decay time of $^4\text{F}_{3/2}$ level of Nd^{3+} , measured at 1057.5 nm (right).

140 3.3. Electric properties

141 The electrical properties were measured for ceramic samples. Frequency dependencies of the real
 142 part of permittivity as a function of Nd^{3+} doping level of the $\text{La}_{1-x}\text{Nd}_x\text{FeO}_3$ nanoceramics were
 143 measured and are shown in Fig. 4. Dotted line corresponds to undoped sample.



144

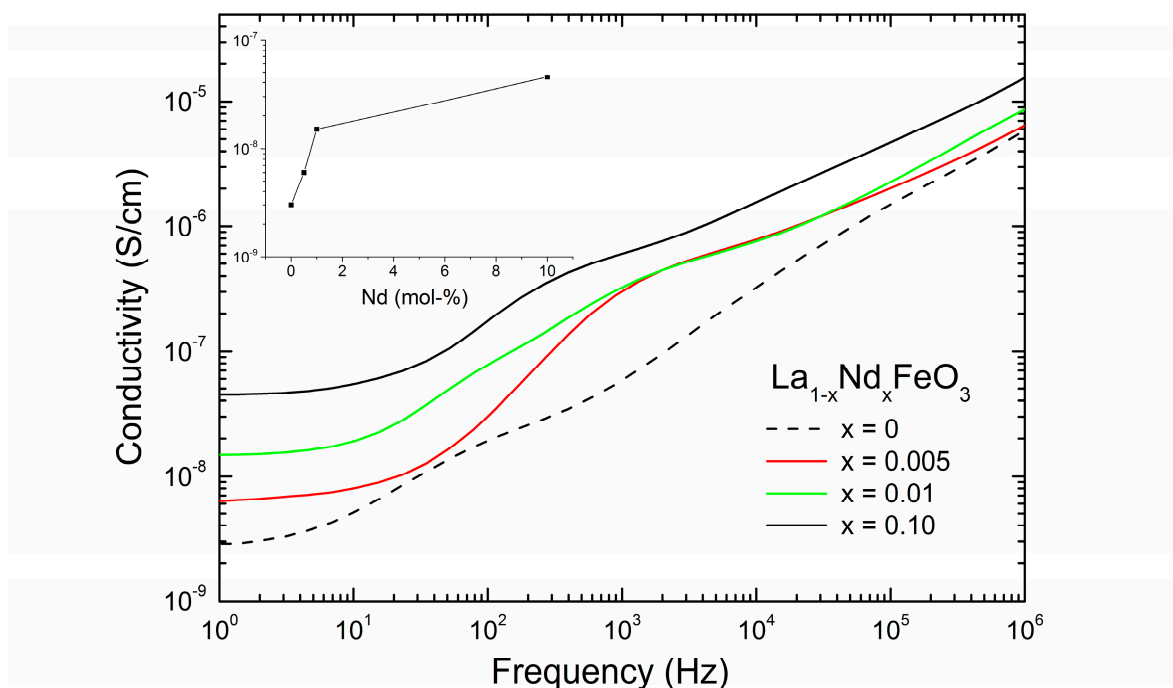
145 **Figure 4.** The real part of permittivity as a function of frequency for $\text{La}_{1-x}\text{Nd}_x\text{FeO}_3$ ceramics.
 146 Dotted line corresponds to the undoped sample.

147 All the samples revealed similar type of dependencies characterized by high values of the dielectric
 148 permittivity. Generally, the values of permittivity increase with doping, as it can be clearly seen for
 149 the samples doped from 0 to 1% of Nd. However, the values of sample doped by 10% of Nd are
 150 lower than those doped by 0.5% and 1%. Furthermore, permittivity of 10% doped sample is lower
 151 than for undoped sample at high frequencies. One of the reasons of such behavior can be an influence

152 of Nd incorporation on the charge transfer. Small amount of Nd can only increase permittivity by
 153 introduction of localized charge carriers. However, at high concentration of Nd, the charge carriers
 154 became partially delocalized thus contributing to the screening of applied electric field especially at
 155 low frequencies.

156 The frequency dependence of conductivity allows to determine the direct influence of charge carriers
 157 doping on the charge transport properties of the nanoceramics (Fig. 5).

158



159

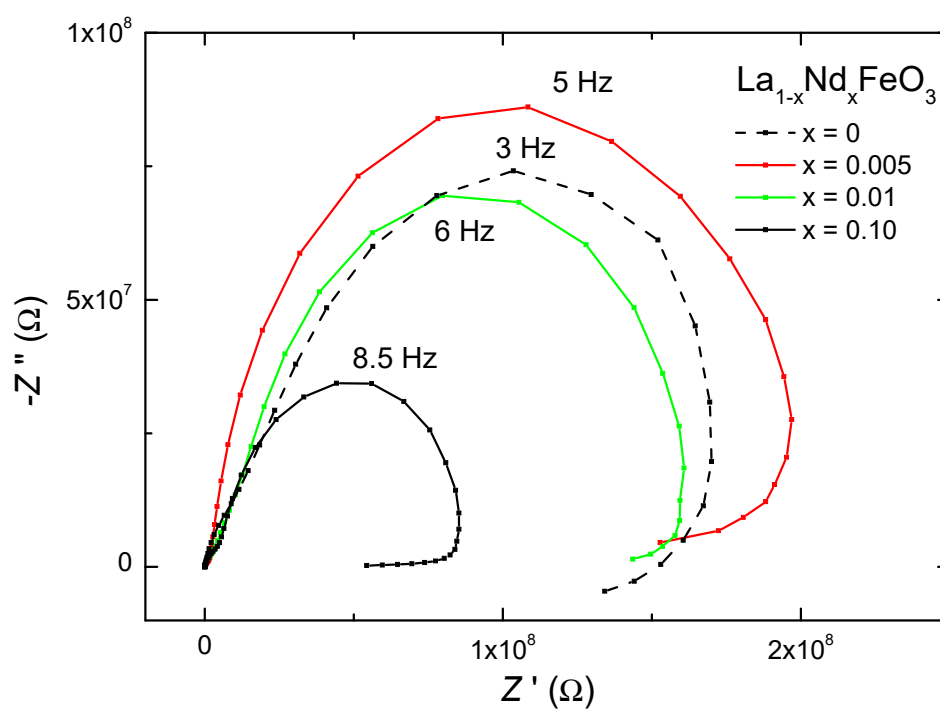
160 **Figure 5.** Frequency dependence of the conductivity of $\text{La}_{1-x}\text{Nd}_x\text{FeO}_3$ ceramics. Dotted line
 161 corresponds to the undoped sample. Inserted figure shows the dc conductivity as a function of
 162 Nd content.

163 The character of dependencies is similar for all the samples suggesting ion conductivity contribution
 164 since conductivity increases with frequency in the whole range. This type of conductivity can be
 165 described by Eq. 1 [19, 20]:

$$166 \quad \sigma'(\omega) = \sigma_0 + A\omega^n, \quad (1)$$

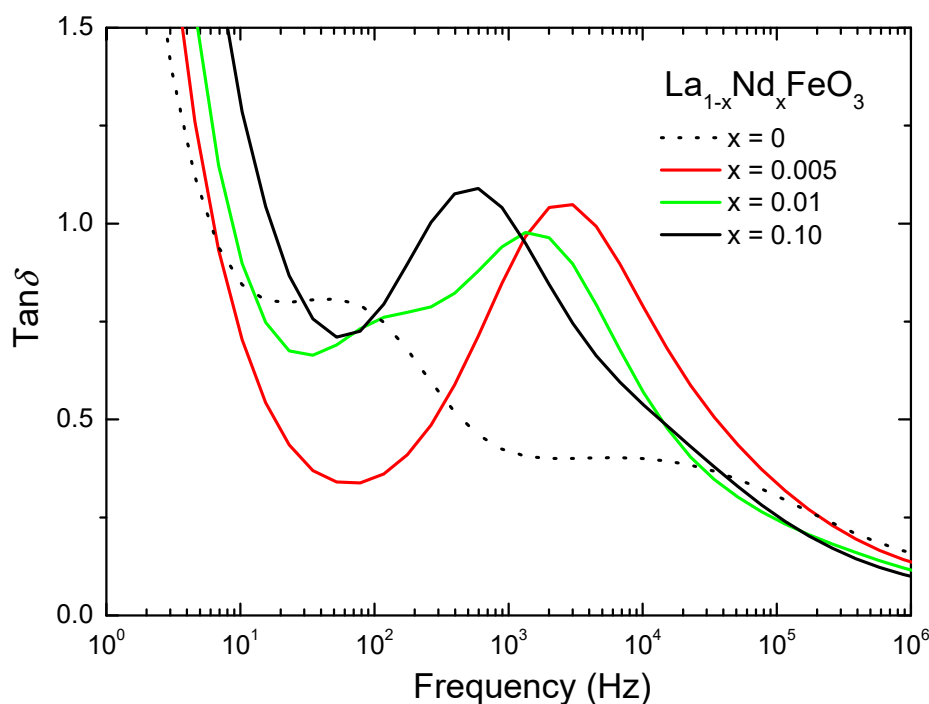
167 where ω is the angular frequency ($\omega = 2\pi f$, f is the frequency of the applied electric field), σ_0 is the dc
 168 conductivity, A is a constant, and $0 < n < 1$. dc conductivity can be estimated from the plateaus at
 169 low frequencies. As it can be seen, the values of dc conductivity increase with doping logarithmically
 170 (see insert in Fig. 5). This is a result of doping by charge carriers. It is worth to note that doping by
 171 10% of Nd^{3+} changes the values of conductivity by an order of magnitude.

172 The simple way to explore the relaxation processes is of the data representation in the Cole-Cole plot
 173 (Fig. 6).



174
 175 **Figure 6.** Cole-Cole plots for the $\text{La}_{1-x}\text{Nd}_x\text{FeO}_3$ ceramics. Dotted line corresponds to the undoped
 176 sample.

177 It is clear that all the samples show relaxation depending on Nd content at low frequencies. The
 178 relaxation frequency increases with amount of Nd. There are also relaxations at high frequencies,
 179 but it is difficult to observe them in presented plots. In order to determine relaxation processes at
 180 high frequencies, the dependencies of loss tangent were analyzed (Fig. 7).

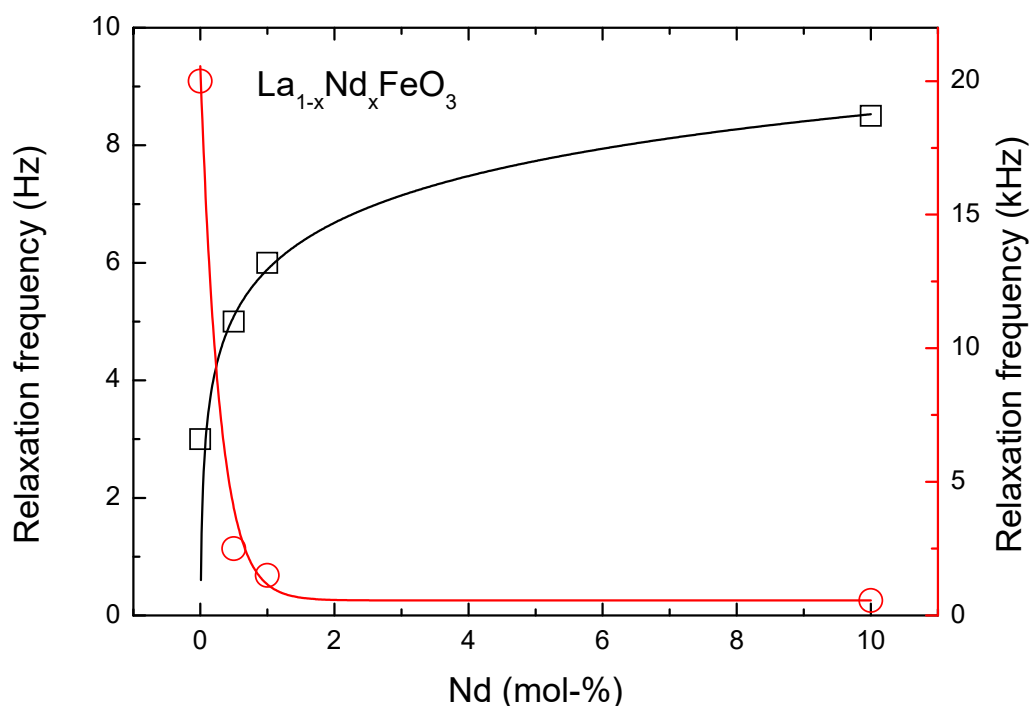


181

182 **Figure 7.** Frequency dependencies of loss tangents of the $\text{La}_{1-x}\text{Nd}_x\text{FeO}_3$ ceramics. Dotted line
183 corresponds to the undoped ceramic.

184 Depending on the doping level, relaxations appear in the wide frequency range. One can see that the
185 frequency of the loss peak systematically decreases with doping. It should be noted that undoped
186 sample revealed two relaxation peaks at 60 Hz and 20 kHz. Similar behavior was observed for 80
187 nm LaFeO_3 sample [21]. In this frequency range, the loss peaks could be explained by the dipole
188 relaxations.

189 A summary of the influence of Nd doping on the relaxation processes and relaxation frequency as a
190 function of Nd concentration is shown in Figure 8.



191

192 **Figure 8.** Relaxation frequency as a function of Nd mol. % content.

193 As it was mentioned above, doping with Nd shifts relaxation frequency to higher frequencies for
 194 low frequency relaxations. However, the increase of relaxation frequency is not linear in this case.
 195 Results of low frequency relaxations can be fitted by the relation (Eq. 2):

$$196 \quad f_0 = 5.88 + 1.15 \ln(n), \quad (2)$$

197 where f_0 is the relaxation frequency; and n is the Nd mol-% concentration. As can be seen, weak
 198 doping has stronger effect than the high one.

199 High frequency relaxation processes have completely opposite character as compared to the low
 200 frequency ones. Increasing of Nd content decreases the relaxation frequency (see red line in Fig. 8).
 201 The values of relaxation frequencies can be fitted by asymptotic exponential dependency (Eq. 3):

$$202 \quad f_0 = 560 + 20\,000 \cdot 0.03^n, \quad (3)$$

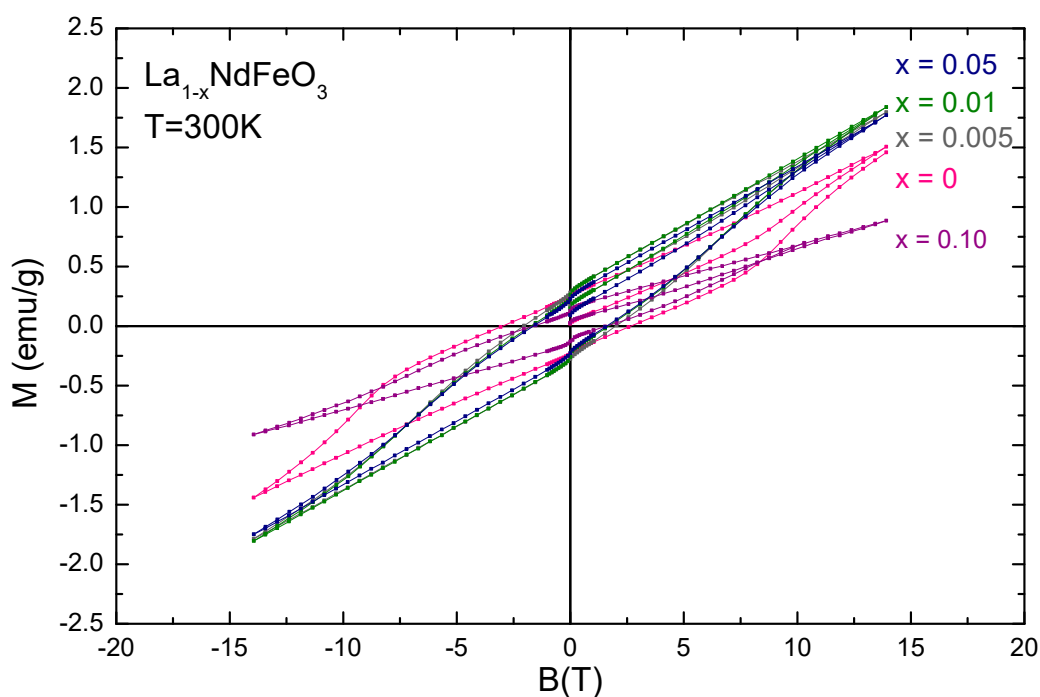
203 Taking into account that low frequencies relaxation is mostly determined by the interfacial and space
 204 charge behavior, whereas high frequency relaxations are results of the dipole interactions, one can
 205 conclude: the Nd doping has an effect on both relaxations and electrical properties of the
 206 nanoceramics that can be adjusted by chemical composition via Eqs. 1 and 2.

207 3.4. Magnetic properties

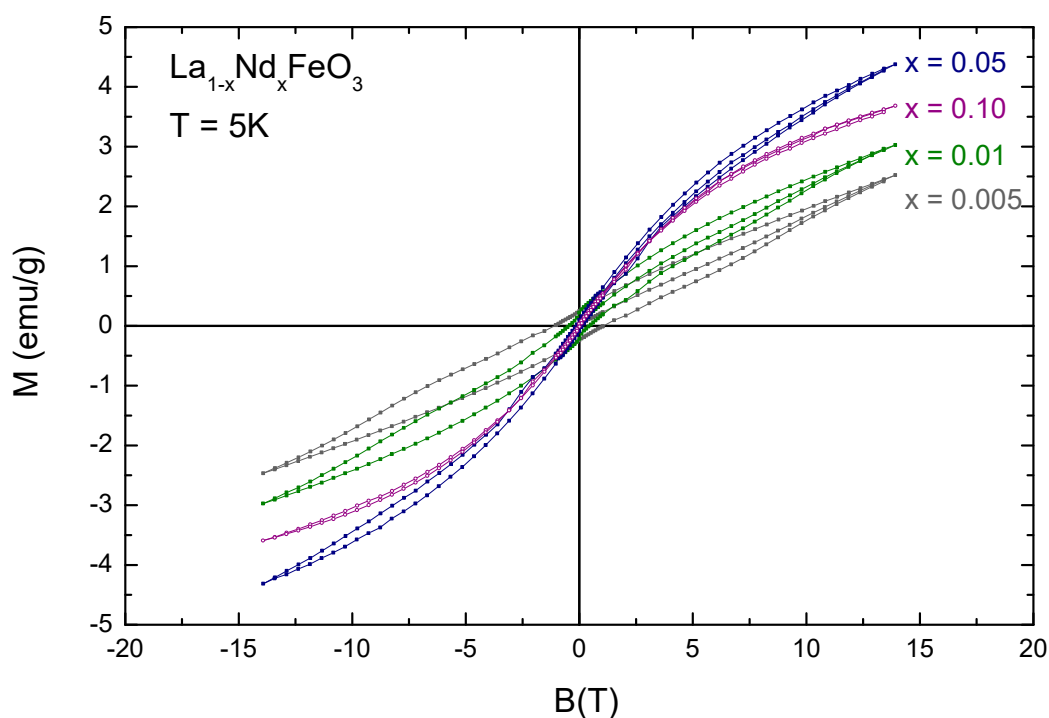
208 Magnetization measurements of the $\text{La}_{1-x}\text{Nd}_x\text{FeO}_3$ ceramics performed at 300 K and 5 K temperatures
 209 have testified an evolution of the magnetic properties as a function of dopant concentration and
 210 temperature (Fig. 9). The $M(H)$ dependencies obtained at room temperature demonstrate a notable
 211 reduction in coercivity of the compounds with increasing dopant concentration. As small as 0.5% of
 212 neodymium concentration significantly modifies magnetic anisotropy of the compounds which
 213 leads to a drastic (40%) reduction in coercivity while a coercive field does not significantly change

214 with further increase of the dopant content in the measured concentration range (up to 10%).
215 Modification in the magnetic structure caused by the chemical substitution also leads to about 15%
216 increase in the in-field magnetization which is most probably associated with an alteration in the
217 chemical bond angle Fe-O-Fe. It should be noted that magnetic structure of the compounds remains
218 to be antiferromagnetic while small ferromagnetic contribution is related to uncompensated surface
219 spins originated from nanoscale crystallites as well as by weak ferromagnetism related to a canting
220 of the magnetic moment associated with Dzyaloshinsky-Moria interactions [22]. An increase in the
221 dopant content up to 10% causes a reduction of ferromagnetic component in the magnetic
222 interactions and compound $\text{La}_{0.9}\text{Nd}_{0.1}\text{FeO}_3$ is characterized by nearly collinear antiferromagnetic
223 structure.

224 Isothermal magnetization measurements performed at 5 K testify a strong reduction in the coercivity
225 of the compounds while magnetic moment becomes notably larger in strong magnetic fields. Strong
226 decrease in the coercive field of the compounds at low temperature is related to spin flip transition
227 occurred in LaFeO_3 -based compounds at about 150 K. A decrease in coercivity of the compounds
228 takes place gradually upon dopant concentration increase thus pointing at progressive alteration of
229 the easy magnetization axis. An increase of magnetization occurred upon the dopant content is most
230 probably caused by positive exchange interactions formed between Fe and Nd ions. An increase in
231 the dopant content above 5% leads to a gradual strengthening of the antiferromagnetic component
232 caused by negative exchange interactions formed between Nd ions, while an in-field magnetization
233 observed for the compound with $x=0.1$ still remains much larger than that observed for the lightly-
234 doped compounds.



235



236

237 **Figure 9.** Field dependencies of magnetization recorded for $\text{La}_{1-x}\text{Nd}_x\text{FeO}_3$ ceramics at room
 238 temperature (top) and at temperature of 5 K (bottom).

239 The compounds having the same nominal chemical compositions as those mentioned above but in
 240 different form (powder and ceramic) are apparently characterized by different magnetic properties.
 241 The compounds in a form of ceramics pieces show gradual increase of room temperature in-field

242 magnetization with Nd content up to 10% while the ground compounds have nearly the same
243 magnetization which remains to be stable regardless of Nd concentration (except for the compound
244 with maximal content of the dopant ions). Gradual increase in the in-field magnetization points at
245 progressive modification of the magnetic properties of the compounds which is most probably
246 associated with an increased contribution from uncompensated spins formed near structural defects.
247 It should be noted that the magnetic structure of the compounds $0 < x < 0.1$ remains unaffected and it
248 is similar to that characteristics for the ground samples. The compounds with $x=0.1$ of both compared
249 series testify an alteration in their magnetic structure expressed as a drastic decrease in the
250 magnetization and coercive field which signifies a strengthening of antiferromagnetic interactions
251 induced by the chemical substitution. The difference of the magnetic properties observed for the
252 compounds in a form of ceramic pellets and ground ones is caused by their different crystalline
253 morphology and defectiveness of the compounds while the magnetic structure remains similar.

254 4. Conclusions

255 In this work we have fabricated and characterized a series of nanopowders and nanoceramics
256 of $\text{La}_{1-x}\text{Nd}_x\text{FeO}_3$ doped with different Nd^{3+} concentration. It was observed that with the increase of
257 doping the unit cell become smaller what have impact on the magnetic and dielectric properties of
258 the nanostructures. In the luminescence spectra we observed concentration quenching due to cross
259 relaxation, energy migration, and thermal depopulation of excited states. Luminescence may be
260 observed only for powder samples because in the ceramics due to change of the color after sintering
261 emission is absorbed by the material. An interesting observation was that magnetization of the $\text{La}_{1-x}\text{Nd}_x\text{FeO}_3$
262 is different for powders and for ceramics. This is caused by internal strains induced by
263 sintering process in nanoceramics. It was also observed that the change of the Nd concentration have
264 impact on the magnetization what is most probably caused by positive exchange interactions formed
265 between Fe and Nd ions. All samples revealed relatively high values of dielectric permittivity, which
266 can be improved by small amount of doping. There were observed ionic and dipole relaxations
267 appeared in different frequency ranges. Ionic relaxation frequency has logarithmic dependence on
268 Nd content, whereas dipole relaxation has an asymptotic exponential one. The most important
269 conclusion is the possibility to adjusting desired electric and magnetic properties of $\text{La}_{1-x}\text{Nd}_x\text{FeO}_3$
270 nanoceramics by changing the concentration of introduced Nd.

271 **Supplementary Materials:** The following are available online, Figure S1. (a)-(d) Topography and (e)-(h) surface
272 potential of $\text{La}_{1-x}\text{Nd}_x\text{FeO}_3$ in dependence of Nd doping degree. (a), (e) 0.5%; (b), (f) 1%; (c), (g) 5%; (d), (h) 10%.

273 **Author Contributions:** powder synthesis, XRD analysis, luminescence studies, writing—original draft
274 preparation P.G.; electric properties measurements analysis, K.O.; ceramic preparation, R.T.; writing—review,
275 A.L.; writing—review, supervision, W.S.; magnetic measurements and analysis, D.K.; AFM measurements, D.A.;
276 morphology analysis and discussion of results, A.K.;

277 **Funding:** This project has received funding from the European Union's Horizon 2020 research and innovation
278 programme under the Marie Skłodowska-Curie grant agreement No 778070 – TransFerr – H2020-MSCA-RISE-
279 2017. Part of the work was developed within the scope of the project CICECO-Aveiro Institute of Materials,
280 POCI-01-0145-FEDER-007679 (FCT Ref. UID /CTM /50011/2013), financed by national funds through the
281 FCT/MEC and when appropriate co-financed by FEDER under the PT2020 Partnership Agreement.

282 **Acknowledgments:** The authors would like to thank Dr. Bogusław Macalik for help in ac impedance
283 measurements.

284 **Conflicts of Interest:** The authors declare no conflict of interest. The funders had no role in the design of the
285 study; in the collection, analyses, or interpretation of data; in the writing of the manuscript, or in the decision to
286 publish the results.

287 References

- 288 1. Nolting, F.; Scholl, A.; Stohr, J.; Seo, J.W.; Fompeyrine, J.; Siegwart, H.; Locquet, J.-P.; Anders, S.; Luning,
289 J.; Fullerton, E.E.; Toney, M.F.; Scheinfeink, M.R.; Padmore, H.A.; *Nature*, **2000**, 405, 767-769, DOI:
290 10.1038/35015515.

- 291 2. Khetre, S.M.; Jadhav, H.V.; Jagadale, P.N.; Kulal, S.R.; Bamane, S.R.; *Adv. Appl. Sci. Res.*, **2011**, *2*, 503-511,
292 3. Bhattacharjee, S.; Rahmedov, D.; Wang, D.; Iiguez, J.; Bellaiche, L.; *Phys. Rev. Lett.*, **2014**, *112*, 147601, DOI:
293 10.1103/PhysRevLett.112.147601
294 4. Kimel, A.V.; Kirilyuk, A.; Hansteen, F.; Pisarev, R.V.; Rasing, T.; *J. Phys.: Condens. Matter*, **2007**, *19*, 043201,
295 DOI: 10.1088/0953-8984/19/4/043201
296 5. Karpinsky, D.V.; Troyanchuk, I.O.; Sikolenko, V.; Efimov, V.; Kholkin, A.L.; *J. Appl. Phys.*, **2013**, *113* (18),
297 187218, DOI: 10.1063/1.4801960
298 6. Karpinsky, D.V.; Troyanchuk, I.O.; Bärner, K.; Szymczak, H.; Tovar, M.; *J. Phys.: Condens. Matter.*, **2005**,
299 *17* (46), 7219, DOI: 10.1088/0953-8984/17/46/006
300 7. Mao, A.J.; Tian, H.; Kuang, X.Y.; Jia, J.W.; Chai, J. S., *RSC Adv.*, **2016**, *6*, 100526-100531, DOI:
301 10.1039/c6ra14791g
302 8. Zhu, Z.; Peelaers, H.; Van de Walle, C.G.; *J. Mater. Chem. A*, **2017**, *5*, 15367-15379, DOI:
303 10.1039/C7TA04330A
304 9. Eibschutz, M.; Shtrikman, S.; Treves, D.; *Phys. Rev.*, **1967**, *156*, 562-577, DOI: 10.1103/PhysRev.156.562
305 10. Coutinho, P.V.; Cunha, F.; Barrozo, P.; *Sol. State Comm.*, **2017**, *252*, 59-63, DOI: 10.1016/j.ssc.2017.01.019
306 11. Phokha, S.; Pinitsoontorn, S.; Maensiri, S.; Rujirawat, S.; *J. Sol-Gel Sci. Technol.*, **2014**, *71*, 333, DOI:
307 10.1007/s10971-014-3383-8
308 12. Acharya, S.; Mondal, J.; Ghosh, S.; Roy, S.K.; Chakrabarti, P.K.; *Mater. Lett.*, **2010**, *64* (3), 415-418, DOI:
309 10.1016/j.matlet.2009.11.037
310 13. Winkler, E.; Zysler, R.D.; Mansilla, M.V.; Fiorani, D.; *Phys. Rev. B*, **2005**, *72*, 132409, DOI:
311 10.1103/PhysRevB.72.132409
312 14. Pechini, M.P.; US Patent, **1967**, 3 330 697.
313 15. Fedyk, R.; Hreniak, D.; Łojkowski, W.; Stręk, W.; Matysiak, H.; Grzanka, E.; Gierlotka, S.; Mazur, P.; *Opt.*
314 *Mater.*, **2007**, *29* (10), 1252-1257, DOI: 10.1016/j.optmat.2006.05.016
315 16. Collins, L.; Kilpatrick, J.I.; Kalinin, S.V.; Rodriguez, B.J.; *Rep Prog Phys.*, **2018**, *81*(8), 086101, DOI:
316 10.1088/1361-6633/aab560
317 17. Selbach, S.M.; Tolchard, J.R.; Fossdal, A.; Grande, T.; *J. Solid State Chem.*, **2012**, *196*, 249-254, DOI:
318 10.1016/j.jssc.2012.06.023
319 18. Gluchowski P.; Strek, W.; *Mater. Chem. Phys.*, **2013**, *140*, 222-227, DOI: 10.1016/j.matchemphys.2013.03.025
320 19. Elliott, S.R.; *Adv. Phys.*, **1987**, *36*, 135-217, DOI: 10.1080/00018738700101971
321 20. Mott, N.F.; Davis, E.; *Electronic Processes in Non-crystalline Materials*, Clarendon: Oxford, England, 1979,
322 pp. 59-62
323 21. Qiu, Y.; Luo, Y.S.; Zou, Z.J.; Tian, Z.M.; Yuan, S.L.; Xi, Y.; Huang, L.Z.; *J. Mater. Sci.: Mater. Electron.*, **2014**,
324 *25*, 760-764, DOI: 10.1007/s10854-013-1642-z
325 22. Ederer, C.; Spaldin, N.A.; *Phys. Rev. B*, **2005**, *71*, 060401, DOI: 10.1103/PhysRevB.71.060401